# Materials Processing in Electron Beam-Generated Plasmas

C. Muratore, S.G. Walton, D. Leonhardt, R.F. Fernsler, and R.A. Meger,
Plasma Physics Division, U.S. Naval Research Laboratory, Washington, DC

**Key Words:** Plasma source, Reactive deposition, Pulsed plasma, Metallization

## ABSTRACT

Electron beam-generated plasmas have been well-characterized and established as highly efficient, easily scalable processing tools that exhibit high plasma densities, relatively large concentrations of reactive ion and neutral species, and allow for remarkable spatial and temporal control of plasma specie fluxes. In this work, *in situ* plasma diagnostics complement materials characterization results to demonstrate the utility of electron beam-generated plasmas with respect to three specific applications: plasma assisted nitriding, reactive sputter deposition and polymer treatment prior to metallization. Plasma assisted nitriding of AISI 316 stainless steel was observed at the rate of 6.7 microns per hour at 415°C in nitrogen-argon plasmas. The nitriding rate was attributed to the composition of the neutral and ionized nitrogen flux to the substrate. The microstructure of reactively sputtered thin films varied with the $N^+/N_2^+$ ion flux ratios, which were manipulated by operating the electron beam generated plasma to increase the atomic nitrogen ion flux. A fluoropolymer (PTFE) treated in electron beam generated oxygen plasmas exhibited modified surface morphologies, and improved adhesion of metallized layers.

## INTRODUCTION

Multiple kilovolt electron beams passing through a 10-65 Pa nitrogen gas background generate plasmas that have demonstrated ion densities between $10^{10}$ and $10^{12}$ $cm^{-3}$, and are capable of delivering large atomic ion fluxes [1]. The composition of the ion flux to a surface in an electron beam generated plasma system can also be varied significantly by adjusting its position relative to the electron beam source [2, 3]. Beam generated plasmas also require less power per electron-ion pair than other plasma generation techniques since most of the energy supplied by the beam electrons is consumed by gas ionization and dissociation reactions rather than by electron heating and gas excitation [4]. In the absence of externally applied fields, plasma electrons are rapidly cooled by inelastic collisions with the background gas, resulting in a low plasma electron temperature (~0.5 eV), and small sheath potentials at electrodes exposed to the plasma [5]. Additionally, plasmas generated by electron beams are easily scalable to large areas and a variety of geometries [6]. Uniform planar plasmas of approximately one square meter are routinely generated with an electron beam source in the Large Area Plasma Processing Systems (LAPPS) developed at the US Naval Research Laboratory.

To demonstrate how processing applications might benefit from the unique features of electron beam-generated plasmas, stainless steel nitriding, reactive film deposition and polymer pretreatment experiments were conducted. The plasma assisted nitriding results illustrate the process control afforded by the electron beam-generated plasma and the role of specific ion and neutral nitrogen species in stainless steel nitriding. The effect of ion flux composition on film microstructure during growth of titanium nitride thin films was also investigated with the electron beam-generated plasma functioning as an auxiliary plasma source during reactive magnetron sputtering. Finally, oxygen electron beam-generated plasmas were used to modify polytetrafluoroethylene (PTFE) surfaces prior to copper and aluminum metallization. The pretreatment resulted in improved metal adhesion.

## EXPERIMENT APPARATUS

All processing experiments were performed in chambers similar to that illustrated schematically in Figure 1, except for the nitriding experiments in which the magnetron was removed. The base pressure for all experiments was 1 x $10^{-3}$ Pa or lower. A hollow cathode driven by 2 millisecond long, -2 kV pulses at different duty cycles was used as the electron beam source. The current supplied to the cathode increased with pressure, and was 3 $mA/cm^2$ or less to generate a 15 cm wide x 60 cm long x 1 cm thick sheet (900 $cm^3$) of high-density plasma. The cross sectional area of the beam was defined by the geometry of the hollow cathode and the grounded slotted anode, and was maintained over the beam length by a 150-165 G magnetic field. The process gases (99.999 pure) were introduced using mass flow controllers, and the operating pressure was regulated by adjusting the flow rate and throttle valve on the vacuum pump as necessary. The 100 $cm^2$ planar sample stage was designed to allow biasing and heating or cooling of the samples, and was also used for quantitative ion flux measurements. The stage was mounted on a linear-motion vacuum feedthrough to allow adjustment of the sub-


© **2004 Society of Vacuum Coaters** 505/856-7188 ISSN 0737-5921
47th Annual Technical Conference Proceedings (April 24–29, 2004) Dallas, TX USA

strate distance relative to the electron beam axis (referred to as *d*). Other application-dependent experimental conditions are described in detail below.

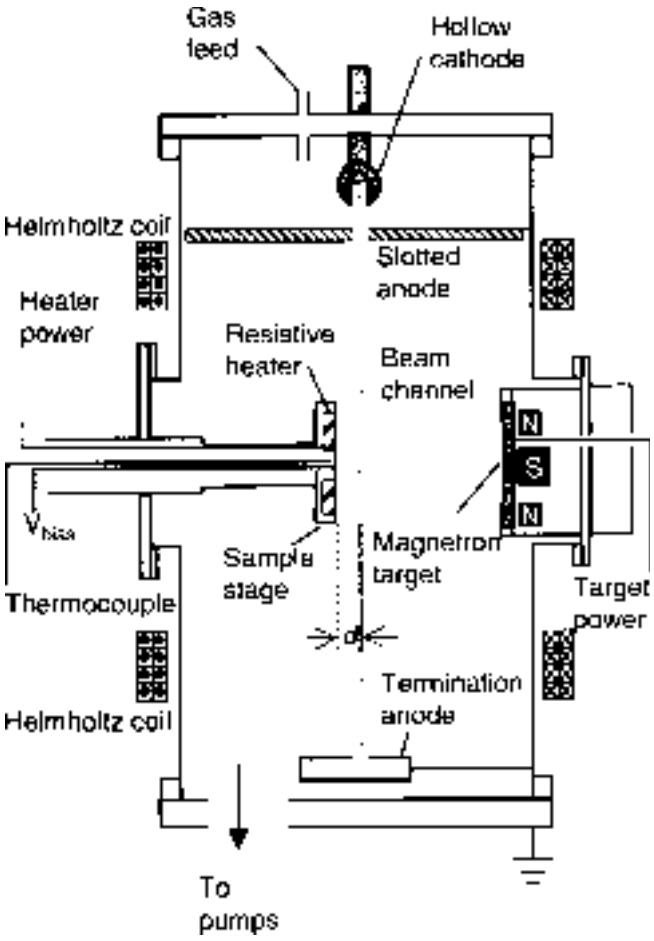


Figure 1: Schematic of the processing chamber. Note that *d* indicates the distance from the substrate to the electron beam axis.

**Plasma Assisted Nitriding**

Samples of 6.5 $cm^2$ electropolished AISI 316 stainless steel were secured to the front of the sample stage shown in Figure 1, heated to 415 ℃ and dc biased to -350 volts for 6.25 hours while exposed to the electron beam-generated plasma. The electron beam was modulated at 500 Hz and 50 percent duty factor. The operating pressure was 21.3 Pa, comprised of 87.5 percent nitrogen and 12.5 percent argon. The exposure time of the substrate to the active phase of plasma production (50% of 6.25 hours) was used to calculate the nitriding rates, which were determined by assuming parabolic diffusion-controlled growth at a rate proportional to the square root of time ($t^{1/2}$) [7,8]. The samples were nitrided under identical conditions at 0.5 cm increments starting at position $d = 1.5$ to 4.0 cm, where $d = 0$ was the center of the beam channel. After nitriding, the specimens were sputter coated with metal while maintained at room temperature and sectioned. The cross sections were then polished and etched in acid to allow observation of the nitrided layer thickness in an optical microscope. The thickness was measured with the cursors of a Vickers microindentor with 0.2 micron resolution.

The EQP analyzer was used to measure the temporally- and spatially-resolved ion energy distributions at a grounded electrode [9], providing relative specie fluxes in plasmas generated under similar conditions as those used in the nitriding experiments. To simulate a substrate bias on the grounded EQP front electrode, the termination anode was dc biased to +100 volts. This voltage raised the plasma potential by 100 volts [10], and created a sheath with an approximate -100 volt potential drop at the front electrode of the EQP analyzer, which was located at $d = 1.5$ cm.

**Reactive Sputtering**

Single crystal (001) silicon substrates were degreased, then loaded into the vacuum chamber at $d = 1.5$ cm, with a target-substrate distance of 7 cm. The substrates were then exposed to an electron beam generated plasma at 50 percent duty in 6 Pa argon. During plasma exposure, the substrates were dc biased to -50 volts, and heated from room temperature to 250 ℃ in 15 minutes. The temperature was maintained for an additional three minutes, then the 15 cm planar titanium magnetron target was powered to 800 Watts. After two minutes of operation in pure argon, 0.9 sccm nitrogen was introduced into the chamber. The target was powered for an additional 20 minutes in the argon-nitrogen gas mixture while the substrate was maintained at 250 ℃, and -50 volts dc. Films were grown with the electron beam source running at 50 percent duty, or turned off. For both experiments, the total time-averaged ion current was held constant (0.6 mA $cm^{-2}$) by adjusting the axial magnetic field to increase or decrease the ion flux from the magnetron, with the ion/metal atom ratio maintained at approximately 2. The microstructure of the two films was then characterized using x-ray diffraction and atomic force microscopy.

**Polymer Pretreatment**

The experimental setup was as shown in Figure 1, with a 1.2 inch diameter planar magnetron equipped with an aluminum or copper sputtering target located 13 cm from the substrates to supply the metal flux. Square samples (2.5 cm on a side) of 70 micron thick PTFE were ultrasonically cleaned in methanol for 15 minutes prior to processing or other testing. The PTFE was then loaded in the chamber on the cooled processing stage and exposed to an oxygen electron beam-generated plasma. After 50 minutes at 20 percent duty in 6.7 Pa pure oxygen at $d = 2.5$ cm, the electron beam source was turned off, the oxygen was pumped away to 1 x $10^{-3}$ Pa, and argon was introduced to the chamber to 2.4 Pa. A 100 Watt magnetron discharge was then initiated to deposit the metal film. Metal films were also deposited under the same conditions on untreated samples of PTFE.

The adhesion of the metal films deposited on the pre-treated PTFE substrates was qualitatively assessed using the Scotch Tape test [11]. The surface morphology of treated and untreated PTFE samples was also examined with an atomic force microscope (AFM). Additionally, the PTFE/water/air contact angle was measured before and after plasma treatment with the equilibrium sessile drop method [11]. The contact angle on the treated PTFE was measured four hours after removal of the sample from the vacuum chamber.

## RESULTS

### Plasma Nitriding

The total positive ion flux collected at the workpiece biased to -350 V decreased linearly with distance from a value of 0.38 mA/cm$^2$ at $d$ = 1.5 cm, to 0.15 mA/cm$^2$ at $d$ = 4.0. The nitriding rate however, increased with distance under certain conditions. Figure 2 shows the nitriding rate normalized to the ion flux. The nitriding rate (normalized or not) exhibits two maxima when plotted against distance, one close to the electron beam ($d$ = 1.5 cm) and a second near $d$ = 3.5 cm, even though the ion flux decreased monotonically with $d$ over this range. The nitriding rate dependence on ion flux reported by Williamson et al. [12] and Brokman et al. [13], were also normalized by ion flux and are shown in Figure 2 for comparison.

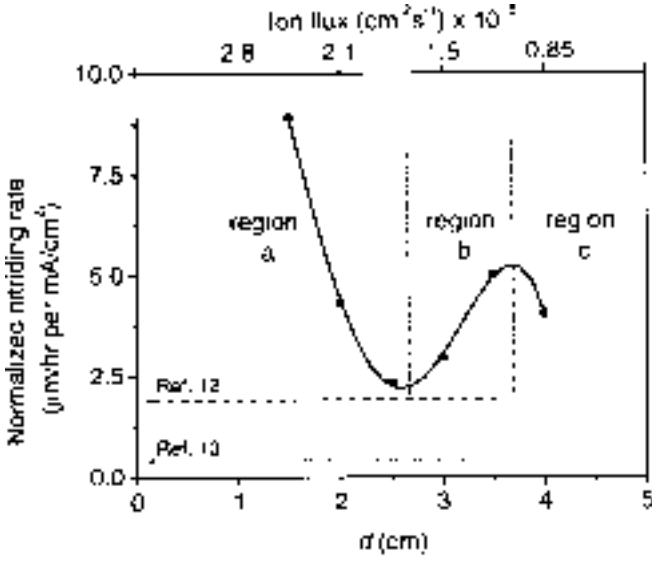


Figure 2: Nitriding rate at different values of $d$ and normalized by the magnitude of the total ion flux for the electron beam-generated plasma. Also shown are normalized nitriding rates from References 6 and 7. The top scale shows how the ion flux changed with distance in the electron beam generated system, and does not correlate to the referenced data.

Figure 3 shows the contribution of each ion specie to the total ion flux integrated over all time measured with the EQP analyzer for different values of $d$. The flux was composed of predominantly $N_2^+$ ions for $d$ < 2.5 cm, while at greater distances most of the flux consisted of $N^+$ ions. Regardless of $d$, the relative fraction of atomic nitrogen ions contributing to the total ion flux was always over 40 percent. The mass-resolved ion energy distributions in Figure 4 show that the molecular nitrogen ions arrived at the EQP electrode with less energy than the atomic ions, which displayed energies commensurate with the imposed -100 V sheath potential.

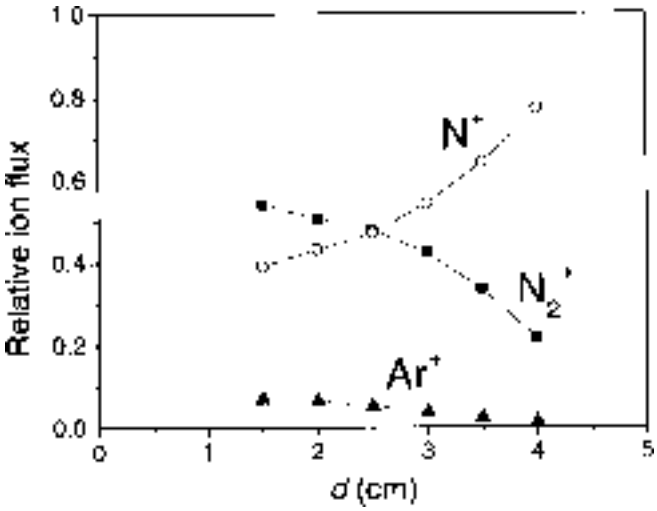


Figure 3: The relative $N_2^+$, $N^+$ and $Ar^+$ fluxes for different values of $d$.

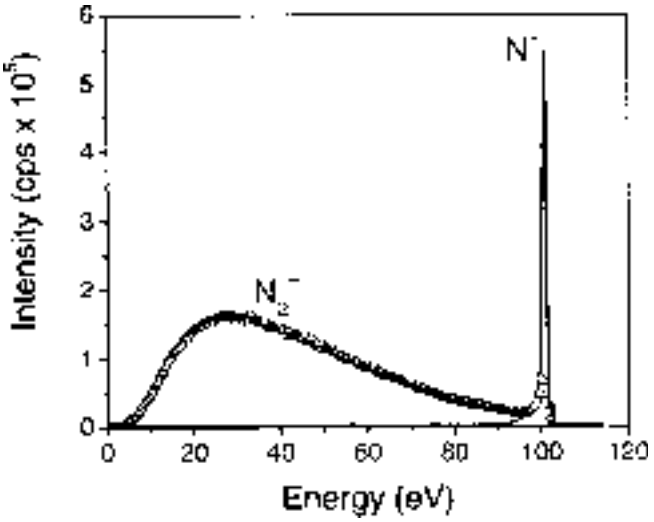


Figure 4: Ion energy distributions for molecular and atomic nitrogen ions incident on an electrode located at $d$ = 1.5 cm and biased to approximately -100 V relative to the plasma.

X-ray diffraction experiments revealed that the nitrided layers contained approximately 30 atomic percent nitrogen, and nano-indentation experiments showed that the hardness of each layer was in excess of 15 GPa. The hardness of the untreated steel was approximately 2.5 GPa.

**Reactive Sputtering**

Films deposited by reactive sputtering were measured to be 150 nm thick, and x-ray diffraction patterns showed that the films were composed of (002) and (111) TiN crystals. Integrated peak intensities showed an increase in $I_{(200)}/(I_{(200)}+I_{(111)})$ from 20 percent to 27 percent when the $N^+/N_2^+$ ion ratio was increased with the electron beam source during deposition. Atomic force micrographs over different 4 $mm^2$ regions of the film surfaces consistently showed that as the $I_{(200)}/(I_{(200)}+I_{(111)})$ ratio increased, the most probable grain height decreased, as shown in Figure 5.

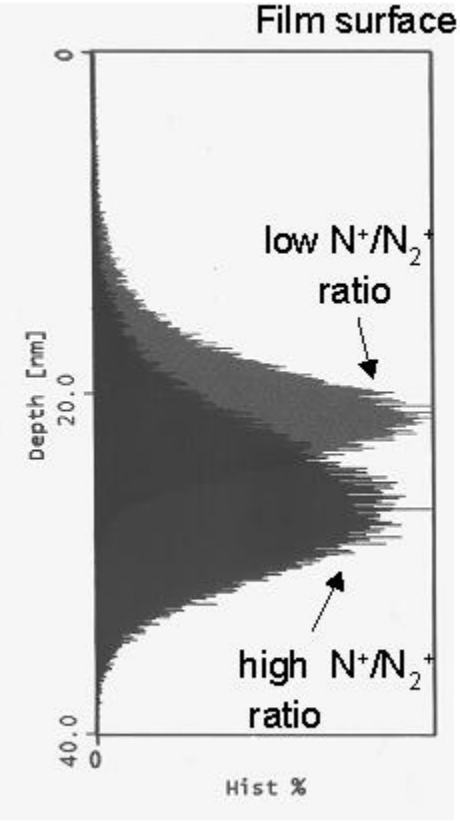


Figure 5: Histograms generated from atomic force microscope data representing the height distributions of TiN islands grown during deposition under different $N^+/N_2^+$ ion flux ratios. A depth of 0 nm corresponds to the film surface.

**Polymer Pretreatment**

Figure 6a and b show the aluminum films deposited on the untreated (a) and treated (b) PTFE substrates after adhesion testing. Both the aluminum and copper films suffered delamination on the untreated PTFE, but remained completely intact on the substrate exposed to the oxygen plasma. Figure 7a and b show atomic force micrographs illustrating the difference in surface morphology of the untreated and treated PTFE substrates. Filament-like structures were observed on the treated sample surface. The water contact angle measurement showed that the oxygen plasma treatment reduced the PTFE/water/air contact angle from 120° to 85°.

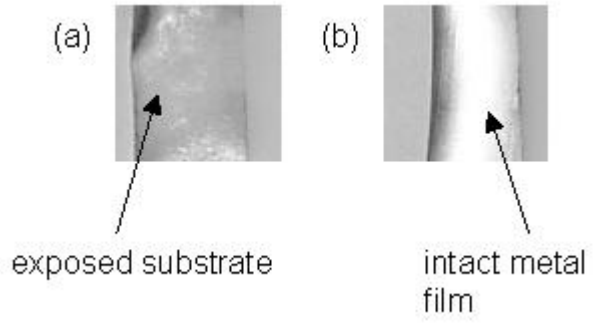


Figure 6: Aluminum films after adhesion testing (a) without pretreatment, and (b) with electron beam generated oxygen plasma pretreatment. The film was almost entirely removed by the adhesion test on the untreated substrate, but unchanged on the treated substrate.

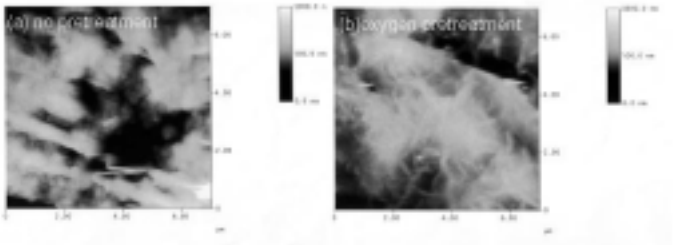

Figure 7: Atomic force micrographs of (a) ultrasonically cleaned PTFE and (b) treated PTFE.

**DISCUSSION**

**Plasma Nitriding**

The large atomic flux produced by the electron beam generated plasma is useful for nitriding of stainless steel, which must be sputtered as it is nitrided to eliminate growth of oxide layers that inhibit the nitriding process [14]. Figure 4 shows that atomic ions accelerate to the full sheath potential, while the molecular ions are only accelerated across part of the sheath, thus implying that most molecular nitrogen ions experience collisions in the plasma sheath, but nearly all the atomic nitrogen ions undergo collisionless transport to the substrate. In stainless steel nitriding systems where molecular nitrogen ions comprise nearly all of the ion flux, operating pressures must be kept low to reduce the frequency of charge exchange collisions, otherwise the energy of the ions will be insufficient to eliminate the constantly regenerating surface oxide. Atomic nitrogen ions have a much longer charge exchange mean free path than the molecular ions [15], and therefore higher nitrogen pressures can be employed for nitriding without impeding oxide sputtering during nitride growth. The increased allowable nitrogen pressure results in higher nitrogen atom fluxes, thereby accelerating the nitriding rate, which is high compared to other processes [16].

In addition to high nitriding rates, the spatial dependence on flux composition found in electron beam generated plasmas provides further insight as to which nitrogen species are active

in the nitriding process. Figure 2 shows that the nitriding rate varied nonlinearly with the total ion flux. Since the rate dependence is known to be linear when the flux composition is constant (as in the other systems shown in Figure 2), it can be presumed that the nitriding rate depended on the composition as well as the magnitude of the ion flux to the substrate in the electron beam system. To better understand the relationship between nitriding rate and flux composition, the number of nitrogen atoms available to diffuse into the substrate resulting from the ion and neutral flux was estimated at each position, $d$ [3]. A comparison of the magnitude of the neutral ($j_N$) and ion ($j_i$) flux at each distance with the observed nitriding rates suggests that the nitriding rate is controlled by $j_i$ when $j_i > j_N$ (as in region a on Figure 2). If $j_i < j_N$ (region b), the nitriding rate is dictated by $j_N$, provided the oxygen sputter rate ($S_o$) is greater than the flux of residual oxygen ($j_O$) during processing. Region c in Figure 2 implies that when $j_O < S_O$, the nitriding rate decreased regardless of the magnitude of $j_N$.

**Reactive Sputtering**

The total flux and ion energy were constant for both deposition experiments, however, the composition of the ion flux was changed with the auxiliary electron beam generated plasma. The increased fraction of (002) oriented crystals associated with the increased atomic nitrogen ion flux is in agreement with the kinetic arguments presented by other authors [17,18]. Gall et al. [17] state that the presence of atomic N on the surface should promote growth of (002) grains over (111) grains during competitive texture evolution. Additionally, grains of (002) oriented TiN have shown faster lateral growth than (111) grains, which rapidly grow normal to the substrate surface [19]. The AFM bearing curves in Figure 5, which show a lower average grain height for the film with more (002) oriented grains, would be consistent with an increased number density of shorter, broader islands. Preferred growth of (002) oriented crystals is typically accompanied by reduced film porosity [19]. Further experimentation is currently underway to further isolate the effects of flux composition on the microstructure and properties of reactively sputtered thin films.

**Polymer Pretreatment**

The atomic force micrographs of the PTFE material in Figure 7 illustrate a change in surface morphology after exposure to the electron beam generated oxygen plasma. The surface is altered from featureless islands to intermingled filaments radiating out from the previously existing islands. Similar structures have been observed by others in purely physical sputtering processes [20] and oxygen ion beam processes [21], however, the ion energies resulting from the beam generated plasma were less than 5 eV [5].

Changing the surface morphology of fluoropolymeric materials has been established as the primary mechanism for increasing adhesion by many authors [22], who have illustrated how the increased surface area of the substrate increases the effective length of the interface, thus giving the film more sites to bond to. Additionally, increased force is necessary to peel the metal film from an angle off the surface normal. The fact that the adhesion of both copper and aluminum films increased with plasma treatment further suggests that modification of surface morphology is the dominant mechanism for improved adhesion, considering that copper is a relatively inert material compared to aluminum [23].

The oxygen plasma also transformed the PTFE from a non-wetting material (q >100°) to wetting, even after exposure to atmosphere for several hours. The reduced surface energy and increased film adhesion could be related to differences in surface morphology or from surface "activation" by exposure to the oxygen plasma. Some authors suggest that plasma treatment results in branching and cross-linking of polymer surfaces [22]. In PTFE, for example, all carbon atoms are found as $CF_2$, except for those at the ends of the chains where three fluorine atoms bond to carbon as $CF_3$. The branching and cross-linking processes, due to plasma treatment, create carbon sites with less fluorine neighbors, or C sites with no fluorine neighbors which could also lead to enhanced metal bonding [24].

## CONCLUSIONS

The unique properties of electron beam-generated plasmas were applied in plasma assisted nitriding, reactive sputtering and polymer metallization processes. The large concentration of atomic nitrogen ions allowed the development of a high rate stainless steel nitriding process. The nitriding rate was also shown to exhibit a dependence on the composition of the nitrogen ion flux in addition to its magnitude. Use of the electron beam source during reactive sputtering revealed that film microstructure depends on ion flux composition, with an increased atomic nitrogen ion flux corresponding to an increase in (002) orientation for TiN. Adhesion of copper and aluminum films was improved with an electron beam generated oxygen plasma pretreatment, and was likely related to the modified surface morphology of the PTFE after oxygen treatment.

With simple scalability to large areas, low ion energies, low power consumption and controllable specie fluxes, electron beam generated plasmas appear to be an attractive option for diverse production and research applications.

## ACKNOWLEDGMENT

This work was supported by the Office of Naval Research. The authors are indebted to Professor J.J. Moore at the Colorado School of Mines for use of the unbalanced magnetron. C.M. is grateful for support from the American Society for Engineering Education.

**REFERENCES**


1. S.G. Walton, D. Leonhardt, C. Muratore, D.D. Blackwell, R.F. Fernsler, and R.A. Meger, "Ion Flux Measurements in Electron Beam-Generated Plasmas," 45th Annual Technical Conference Proceedings of the Society of Vacuum Coaters, 382, 2002.
2. S.G. Walton, C. Muratore, D. Leonhardt, D.D. Blackwell, R.F. Fernsler, and R.A. Meger, "Electron Beam-Generated Plasmas for Materials Processing," submitted to Surface Coatings and Technology, Sept. 2003.
3. C. Muratore, S.G. Walton, D. Leonhardt, R.F. Fernsler, D.D. Blackwell, and R.A. Meger, "The effect of plasma flux composition on the nitriding rate of stainless steel," submitted to Journal of Vacuum Science and Technology, Nov. 2003.
4. R.F. Fernsler, W.M. Manheimer, R.A. Meger, J. Mathew, D. P. Murphy, R.E. Pechacek, and J.A. Gregor, "Production of large-area plasmas by electron beams," Phys. of Plasmas, 5, 2137, 1998.
5. D. Leonhardt, S.G. Walton, D.D. Blackwell, W.E. Amatucci, D.P. Murphy, R.F. Fernsler, and R.A. Meger, "Plasma diagnostics in large area plasma processing system," J. Vac. Sci. Technol., 19, 1367, 2001.
6. R.A. Meger, D.D. Blackwell, R.F. Fernsler, M. Lampe, D. Leonhardt, W.M. Manheimer, D.P. Murphy, and S.G. Walton, "Beam-generated plasmas for processing applications," Phys. of Plasmas, 8, 2558, 2001.
7. D.L. Williamson, O. Ozturk, R. Wei, and P.J. Wilbur, "Metastable phase formation and enhanced diffusion in f.c.c. alloys under high dose, high flux nitrogen implantation at high and low ion energies," Surf. Coat. Technol., 65, 15, 1994.
8. T. Czerwiec, N. Renevier, and H. Michel, "Low-temperature plasma-assisted nitriding," Surf. Coat. Technol., 131, 267, 2000.
9. S. G. Walton, D. Leonhardt, D.D. Blackwell, R.F. Fernsler, D.P. Murphy, and R.A. Meger, "Time-resolved ion flux measurements in pulsed, electron-beam-generated plasmas," Phys. Rev. E, 65, 046412, 2002.
10. J.W. Coburn and E. Kay, "Positive-ion bombardment of substrates in rf diode glow discharge sputtering," J. Appl. Phys., 43, 4695, 1972.
11. E. M. Mount II, ed., Association of Industrial Metallizers, Coaters and Laminators (AIMCAL) Metallizing Technical Reference, 3rd Edition, 2001.
12. D.L. Williamson, J.A. Davis, P.J. Wilbur, J.J. Vajo, R. Wei, and J.N. Matossian, "Relative roles of ion energy, ion flux, and sample temperature in low-energy nitrogen ion implantation of Fe-Cr-Ni stainless steel," Nuc. Inst. Met. Phys. Res. B, 127/128, 930, 1997.
13. A. Brokman and F.R. Tuler, "A study of the mechanisms of ion nitriding by the application of a magnetic field," J. Appl. Phys., 52, 468, 1981.
14. S. Parascandola, O. Kruse, E. Richter, and W. Moeller, "Nitriding stainless steels at moderate temperature: Time- and depth-resolved characterization of the near surface composition during the nitriding process," J. Vac. Sci. Technol. B, 17, 855, 1999.
15. A.V. Phelps, "Cross Sections and Swarm Coefficients for Nitrogen Ions and Neutrals in $N_2$ and Argon Ions and Neutrals in Ar for Energies from 0.1 eV to 10 keV," J. Phys. Chem. Ref. Data, 20, 557, 1991.
16. C. Muratore, D. Leonhardt, S.G. Walton, D.D. Blackwell, R.F. Fernsler, and R.A. Meger, "Low Temperature Nitriding of Stainless Steel in an Electron Beam Generated Plasma," accepted for publication by Surface Coatings and Technology, Feb. 2004.
17. D. Gall, S. Kodambaka, M.A. Wall, I. Petrov, and J.E. Greene, "Pathways of atomistic processes on TiN(001) and (111) surfaces during film growth: an ab initio study," J. Appl. Phys., 93, 9086, 2003.
18. C.-S. Shin, S. Rudenja, D. Gall, N. Hellgren, T.-Y. Lee, I. Petrov, and J.E. Greene, Growth, surface morphology, and electrical resistivity of fully strained substoichiometric epitaxial $TiN_x$ layers on MgO(001)," J. Appl. Phys., 95, 356, 2004.
19. J.-S. Chun, I. Petrov, and J.E. Greene, "Dense fully 111-textured TiN diffusion barriers: Enhanced lifetime through microstructure control during layer growth," J. Appl. Phys., 86, 3633, 1999.
20. C-A. Chang, J.E.E. Baglin, A.G. Schrott, and K.C. Lin, "Enhanced Cu-Teflon adhesion by presputtering prior to the Cu deposition," Appl. Phys. Lett., 51, 103, 1987.
21. M. Gheorghiu, G. Popa, M. Pascu, and C. Vasile, "Chemical and Physical Surface Modifications of Polymers by Ion Beam Treatments," in Metallized Plastics, K.L. Mittal ed. p. 269, Marcel Dekker, New York, 1998.
22. C-A. Chang, Y.-K. Kim, and S.S. Lee, "Adhesion of Metals to Fluorocarbon Polymers," in Metallized Plastics, K.L. Mittal ed. p. 345, Marcel Dekker, New York, 1998.
23. T.C. Chen and S.M. Mukhopadhyay, "Metallization of electronic polymers: A comparative study of polyvinylidene, fluoride, polytetrafluoroethylene, and polyethylene," J. Appl. Phys., 78, 5422, 1995.
24. D.R. Wheeler and S.V. Pepper, "Improved adhesion of Ni films on x-ray damaged polytetrafluoroethylene," J. Vac. Sci. Technol., 20, 442, 1995.